HHS Public Access

Author manuscript

Clin Cancer Res. Author manuscript; available in PMC 2021 September 22.

Published in final edited form as:

Clin Cancer Res. 2019 April 15; 25(8): 2560–2574. doi:10.1158/1078-0432.CCR-18-0432.

CAR T Cells Targeting B7-H3, a Pan-Cancer Antigen, Demonstrate Potent Preclinical Activity Against Pediatric Solid Tumors and Brain Tumors

Robbie G. Majzner[1], **Johanna L. Theruvath**[1], **Anandani Nellan**[2], **Sabine Heitzeneder**[1], **Yongzhi Cui**[3], **Christopher W. Mount**[4], **Skyler P. Rietberg**[1], **Miles H. Linde**[5,6], **Peng Xu**[1], **Christopher Rota**[3], **Elena Sotillo**[1], **Louai Labanieh**[7], **Daniel W. Lee**[8], **Rimas J. Orentas**[9], **Dimiter S. Dimitrov**[10], **Zhongyu Zhu**[11], **Brad St Croix**[12], **Alberto Delaidelli**[13,14], **Alla Sekunova**[13,14], **Ezio Bonvini**[15], **Siddhartha S. Mitra**[2,16], **Martha M. Quezado**[17], **Ravindra Majeti**[6,18,19], **Michelle Monje**[4], **Poul H.B. Sorensen**[13,14], **John M. Maris**[20], **Crystal L. Mackall**[1,18,19]

[1]Department of Pediatrics, Stanford University School of Medicine, Palo Alto, California.

[2]Department of Pediatrics, University of Colorado, Denver Anschutz Medical Center, Denver, Colorado.

[3]Pediatric Oncology Branch, NCI, Bethesda, Maryland.

[4]Department of Neurology, Stanford University School of Medicine, Palo Alto, California.

[5]Immunology Graduate Program, Stanford University School of Medicine, Palo Alto, California.

[6]Institute for Stem Cell Biology and Regenerative Medicine, Palo Alto, California.

[7]Department of Bioengineering, Stanford University School of Medicine, Palo Alto, California.

[8]Division of Pediatric Hematology/Oncology, Department of Pediatrics, University of Virginia, Charlottesville, Virginia.

[9]Department of Pediatrics, University of Washington School of Medicine, Seattle, Washington.

Corresponding Author: Crystal L. Mackall, Stanford University, 265 Campus Dr G3141A, MC5456, Stanford, CA 94305. Phone: 650-725-2553; Fax: 650-724-1164; cmackall@stanford.edu.

J.L. Theruvath, A. Nellan, and S. Heitzeneder are the co-second authors and contributed equally to this article.

Authors' Contributions

Conception and design: R.G. Majzner, Y. Cui, R.J. Orentas, D.S. Dimitrov, C.L. Mackall

Development of methodology: R.G. Majzner, Y. Cui, C.W. Mount, L. Labanieh, D.W. Lee, R.J. Orentas, P.H.B. Sorensen, C.L. Mackall

Acquisition of data (provided animals, acquired and managed patients, provided facilities, etc.): R.G. Majzner, J.L. Theruvath, A. Nellan, S. Heitzeneder, Y. Cui, C.W. Mount, S.P. Rietberg, M.H. Linde, P. Xu, C. Rota, R.J. Orentas, Z. Zhu, B.S. Croix, A. Delaidelli, R. Majeti, M. Monje, P.H.B. Sorensen, J.M. Maris

Analysis and interpretation of data (e.g., statistical analysis, biostatistics, computational analysis): R.G. Majzner, J.L. Theruvath, S. Heitzeneder, Y. Cui, C.W. Mount, S.P. Rietberg, C. Rota, E. Sotillo, R.J. Orentas, A. Delaidelli, S.S. Mitra, M.M. Quezado, P.H.B. Sorensen, J.M. Maris, C.L. Mackall

Writing, review, and/or revision of the manuscript: R.G. Majzner, J.L. Theruvath, S. Heitzeneder, Y. Cui, C. Rota, E. Sotillo, D.W. Lee, R.J. Orentas, D.S. Dimitrov, B.S. Croix, E. Bonvini, S.S. Mitra, M.M. Quezado, M. Monje, P.H.B. Sorensen, J.M. Maris, C.L. Mackall

Administrative, technical, or material support (i.e., reporting or organizing data, constructing databases): R.G. Majzner, J.L. Theruvath, S. Heitzeneder, C.W. Mount, P. Xu, C. Rota, A. Sekunova, E. Bonvini, S.S. Mitra, C.L. Mackall

Study supervision: D.W. Lee, S.S. Mitra, M. Monje, C.L. Mackall

Other (provided critical reagents and information): E. Bonvini

Note: Supplementary data for this article are available at Clinical Cancer Research Online (http://clincancerres.aacrjournals.org/).

[10]Center for Antibody Therapeutics, University of Pittsburgh Medical School, Pittsburgh, Pennsylvania.

[11]Cancer and Inflammation Program, NCI, NIH, Frederick, Maryland.

[12]Tumor Angiogenesis Unit, Mouse Cancer Genetics Program (MCGP), NCI, NIH, Frederick, Maryland.

[13]Department of Pathology and Laboratory Medicine, University of British Columbia, Vancouver, British Columbia, Canada.

[14]Department of Molecular Oncology, British Columbia Cancer Agency, Vancouver, British Columbia, Canada.

[15]MacroGenics, Inc., Rockville, Maryland.

[16]Department of Neurosurgery, Stanford University School of Medicine, Palo Alto, California.

[17]Laboratory of Pathology, Center for Cancer Research, NCI, NIH, Bethesda, Maryland.

[18]Department of Medicine, Stanford University School of Medicine, Palo Alto, California.

[19]Stanford Cancer Institute, Stanford University School of Medicine, Palo Alto, California.

[20]Children's Hospital of Philadelphia and Department of Pediatrics, University of Pennsylvania, Philadelphia, Pennsylvania.

Abstract

Purpose: Patients with relapsed pediatric solid tumors and CNS malignancies have few therapeutic options and frequently die of their disease. Chimeric antigen receptor (CAR) T cells have shown tremendous success in treating relapsed pediatric acute lymphoblastic leukemia, but this has not yet translated to treating solid tumors. This is partially due to a paucity of differentially expressed cell surface molecules on solid tumors that can be safely targeted. Here, we present B7-H3 (CD276) as a putative target for CAR T-cell therapy of pediatric solid tumors, including those arising in the central nervous system.

Experimental Design: We developed a novel B7-H3 CAR whose binder is derived from a mAb that has been shown to preferentially bind tumor tissues and has been safely used in humans in early-phase clinical trials. We tested B7-H3 CAR T cells in a variety of pediatric cancer models.

Results: B7-H3 CAR T cells mediate significant antitumor activity *in vivo*, causing regression of established solid tumors in xenograft models including osteosarcoma, medulloblastoma, and Ewing sarcoma. We demonstrate that B7-H3 CAR T-cell efficacy is largely dependent upon high surface target antigen density on tumor tissues and that activity is greatly diminished against target cells that express low levels of antigen, thus providing a possible therapeutic window despite low-level normal tissue expression of B7-H3.

Conclusions: B7-H3 CAR T cells could represent an exciting therapeutic option for patients with certain lethal relapsed or refractory pediatric malignancies, and should be tested in carefully designed clinical trials.

Translational Relevance

We have undertaken the largest screen to date of B7-H3 expression on pediatric solid tumors and CNS malignancies. Using a previously described binder that preferentially binds tumor B7-H3 with restricted recognition on normal human tissues (MGA271, enoblituzumab), we generated a novel second-generation chimeric antigen receptor (CAR). B7-H3 CAR T cells show significant *in vivo* activity against a range of xenograft models of lethal childhood cancers, including orthotopic models of osteosarcoma, Ewing sarcoma, and medulloblastoma. B7-H3 CAR T cells preferentially target tumor cells with high B7-H3 expression, demonstrating a possible therapeutic window for this novel agent. This work merits translation to the clinic where patients who have relapsed pediatric tumors have few therapeutic options, but will require carefully designed studies to mitigate potential toxicity.

Introduction

Great progress has been made in the treatment of childhood cancer over the past 40 years through the use of multimodal therapy, including combination chemotherapy, surgery, and radiotherapy (1). However, these gains have largely been realized in patients with leukemias, lymphomas, and localized sarcomas, while those with high risk and metastatic solid tumors and many CNS malignancies have seen few improvements (2, 3). Furthermore, mortality rates are >90% for nearly all pediatric patients with relapsed sarcomas and brain tumors (4, 5). Attempts have been made to integrate new targeted drugs into the treatment of metastatic or relapsed diseases, but thus far, this approach has not improved outcomes (6, 7). New therapies are desperately needed for children and young adults with high-risk and recurrent solid or CNS tumors.

Immunotherapy represents a growing field of oncology that has already shown impressive results in both children and adults. The use of T-cell checkpoint inhibitors for diseases such as metastatic melanoma has resulted in long-term remissions in previously incurable adult diseases by unleashing a native immune response (8). However, early trials of checkpoint inhibitors have not been promising in most pediatric cancers (9). Limited numbers of neoantigens in these tumors may preclude them from being effectively treated by checkpoint inhibition (10). Consistent with this, we have shown limited expression of PD-L1, a biomarker for response to anti-PD-1 checkpoint blockade, on pediatric solid tumors (11). In contrast, genetically engineered immunotherapeutics can mediate antitumor effects against cancers with low mutational burden, and thus may be more effective against pediatric solid tumors (10).

Chimeric antigen receptor (CAR) T cell therapy is an exciting approach that draws on molecular biology to arm cytolytic T cells with a receptor that can recognize a surface protein on tumor cells (12). CD19 CAR T cells have shown unprecedented results in the treatment of pediatric hematologic malignancies (13–15), but clinical results for solid tumors have thus far not been as remarkable (16, 17). This may relate, in part, to the selection of antigens that have been targeted using CAR T cells for solid tumors. Unlike CD19 and CD22, lineage-derived antigens that are highly expressed on cancer cells (13), many solid tumor antigens are expressed at lower levels on the surface of cancer cells (18). We and others have shown that low-density antigen expression is insufficient for optimal

CAR activation, raising the prospect that low levels of expression on normal tissue may be tolerable (18–21). Uncovering surface targets with differential expression between tumor and normal tissue has been a major focus for the application of CAR T cells outside of hematologic malignancies (22).

B7-H3 (CD276) is a checkpoint molecule expressed at high levels on pediatric solid tumors, including sarcomas and brain tumors (23–25). B7-H3 expression contributes to tumor immune evasion (26) and metastatic potential (27) and is correlated with poor prognosis (28). Two mAbs targeting tumor-associated B7-H3, 8H9 and MGA271, are safe and have generated promising results in clinical trials (29–33). Given its role in tumor biology and its high level of expression across a wide range of pediatric cancer histologies, we hypothesized that B7-H3 would be a good target for CAR T-cell immunotherapy. Here we present our results in constructing and testing a CAR targeting B7-H3, which demonstrates clear evidence of *in vivo* preclinical activity, regressing and clearing osteosarcoma, Ewing sarcoma (EWS), and medulloblastoma xenografts. In addition, we demonstrate that B7-H3 CAR T cells exhibit a therapeutic window through which they may target high antigen–expressing cells while leaving low antigen–expressing cells largely intact.

Materials and Methods

Primary tumor samples

Archived samples representing a variety of pediatric tumor types were obtained from multiple sources (Children's Hospital of Philadelphia, Seattle Children's Hospital, Toronto Sick Kids, and the Children's Oncology Group) as tumor microarrays (TMA). Each TMA comprised of 0.6-mm or 1-mm cores in duplicate. Two slides containing patient diffuse intrinsic pontine glioma (DIPG) samples from 22 patients were obtained from the Pediatric Oncology Branch at the NCI. Informed consent was obtained from all subjects or their guardians for use of their samples for research, and local Institutional Review Boards confirmed that this analysis did not constitute human subjects research.

Immunohistochemistry (IHC) and H-scores

Freshly cut tissue and formalin-fixed, paraffin-embedded TMA sections were analyzed for B7-H3 expression. All IHC was performed using the Ventana Discovery platform. B7-H3 IHC was optimized and performed with an R&D Systems antibody (catalog number AF1027, goat polyclonal antibody) against B7-H3 with 1:1,000 and 1:600 dilution. In brief, tissue sections were incubated in Tris EDTA buffer (cell conditioning 1; CC1 standard) or at 95°C for 36 minutes to retrieve antigenicity, followed by incubation with a respective primary antibody for 2 hours and no heat. Bound primary antibodies were incubated with rabbit anti-goat secondary antibodies (Jackson Laboratories, catalog number 305-005-045, with 1:500 dilution), followed by Ultramap anti-Rabbit HRP and Chromomap DAB detection.

For staining optimization and to control for staining specificity, kidney tissue was used as a negative control and liver tissue was used as a positive control. Intensity scoring was done on a common four-point scale. Descriptively, 0 represents no staining, 1 represents

low but detectable degree of staining, 2 represents clearly positive staining, and 3 represents strong expression. B7-H3 expression was quantified as an H-Score, the product of staining intensity, and % of stained cells.

Cells and culture conditions

Human cell lines used in these studies were supplied by the following sources: MG63.3 by C. Khanna (NCI, NIH, Bethesda, MD), K562 by C. Thiele (NCI, NIH, Bethesda, MD), EW8 by L. Helman (NCI, NIH, Bethesda, MD), NALM6-GL by S. Grupp (University of Pennsylvania, Philadelphia, PA), DAOY and D283 by A. Martin (Johns Hopkins University, Baltimore, MD), D425 by S. Chesier (Stanford University, Stanford, CA), and 293GP and 293T by the Surgery Branch (NCI, NIH, Bethesda, MD). SU-DIPG VI and SU-DIPG XVII were generated as described previously (34). STR fingerprinting was conducted to verify the identity of all cell lines, and each cell line was validated to be *Mycoplasma* free by qPCR or MycoAlert (Lonza). The 293GP and 293T cell lines were cultured in DMEM. For the DIPG cultures, neurosphere-generating cultures were maintained in serum-free media supplemented with B27 (Thermo Fisher Scientific), EGF, FGF, PDGF-AA, PDGF-BB (Shenandoah Biotechnology), and Heparin (StemCell Technologies). D425 cells were maintained in serum-free media supplemented with B27 (Thermo Fisher Scientific), EGF, FGF (Shenandoah Biotechnology), human recombinant LIF (Millipore), and Heparin (StemCell Technologies). All other cells were cultured in RPMI1640. DMEM and RPMI1640 media were supplemented with 2 mmol/L L-glutamine, 10 mmol/L HEPES, 100 U/mL penicillin, 100 μg/mL streptomycin (Invitrogen), and 10% heat-inactivated FBS.

PBMC and T-cell isolation

Elutriated human peripheral blood mononuclear cells (PBMC) from consenting, healthy donors were obtained from the Department of Transfusion Medicine, NIH Clinical Center, under an NIH institutional review board–approved protocol, and cryopreserved. Thawed PBMCs were cultured in AIM-V media (Invitrogen) supplemented with 2 mmol/L L-glutamine, 10 mmol/L HEPES, 100 U/mL penicillin, 100 μg/mL streptomycin, 5% heat-inactivated FBS, and r-human IL2 (PeproTech). PBMCs were used for the majority of experiments. For the D425 and EW8 *in vivo* experiments, isolated T cells were obtained by negative selection using a RosetteSep T cell Isolation Kit (Stem Cell Technologies) on buffy coats obtained from the Stanford Blood Center.

Identification of B7-H3 single-chain variable fragments

A yeast display naïve, single-chain variable fragment (scFv) human antibody library was used to generate the anti-human CD276 scFvs as described previously (35). The library was constructed using a collection of human antibody gene repertoires, including the genes used for the construction of a phage display Fab library and those from more than 50 additional individuals and contained a total of 1e10 scFvs. *In vitro* selection of the yeast display library involved three rounds of sequential panning on biotinylated, purified recombinant CD276(ED)-AP (alkaline phosphatase) fusion proteins. For this, 10 μg of biotinylated hCD276(ED)-AP was incubated with approximately 5e10 cells from the initial naïve antibody library in 50 mL PBSA (PBS containing 0.1% BSA) for 2 hours, washed with PBSA, and captured with streptavidin-conjugated microbeads from Miltenyi Biotec using

the AutoMACS system. The sorted cells were amplified and the panning was repeated once with the human hCD276 (ED)-AP and once with the mouse mCD276(ED)-AP protein to enrich for cross-reactive binders. After characterizing several scFvs for binding specificity, cross-species reactivity, a panel of five binders (1–5) were sequenced and used for CAR construction.

B7-H3 CAR construct synthesis

B7-H3 scFvs (five from the yeast display library and one provided by MacroGenics (Rockville, MD) were codon optimized for expression in human cells and synthesized by GeneArt (Life Technologies), and then introduced into an MSGV.1 retroviral expression vector containing a CD8-α hinge-transmembrane domain, a CD137 (4-1BB) costimulatory motif, and a CD3ζ signaling domain. The best performing CARs were also tested in a construct containing both the 4-1BB and CD28 costimulatory motifs and a CD3ζ signaling domain (third-generation CAR). Where indicated, the sequence of the human IgG1 constant domain (CH2-CH3) was inserted between the scFv and the transmembrane domain. Resultant B7-H3 CAR constructs were sequence verified (Macrogen) and used for downstream applications. Both the B7-H3 CAR and the CD19 CAR were fused to mCherry at the C terminus end for T-cell trafficking experiments as described previously (36).

Production of retroviral supernatant and CAR T-cell transduction

Retroviral supernatant for the B7-H3 CARs or CD19 CARs was produced by transient transfection of 293GP cells with the corresponding CAR plasmid and an RD114 envelope plasmid as described previously (18). T-cell transduction was performed as described previously (18). Briefly, PBMCs were thawed and activated by culture for 2 or 3 days in the presence of 40 U/mL rhIL2 (PeproTech) and anti-CD3/CD28 beads (Dynabeads, Human T-Activator CD3/CD28, Life Technologies) at a 3:1 bead:T-cell ratio. Cells were exposed to retrovirus-containing supernatants on days 2 and 3, or days 3 and 4, in media containing 300 U/mL rIL2 on retronectin-coated nontissue culture plates (on plate method as per manufacturer, Takara/Clonetech). Beads were magnetically removed on day 4 or 5, and cells expanded in AIM-V media containing 300 U/mL IL2 until use *in vitro* and *in vivo*. For both *in vivo* and *in vitro* assays, CAR T cells were used on day 3–5 after bead removal.

Lentiviral engineering of tumor cell lines

NALM6-GL (GFP-Luciferase) cell lines stably overexpressing B7-H3 were produced by lentiviral transduction with supernatant containing the cDNA for B7-H3 (Origene, RC215064L1). The resultant bulk population was stained using B7-H3 antibody (R&D Systems, clone MAB1027) and sorted into high-, medium-, and low-expressing lines using a FACS Aria (BD Biosciences). The bulk populations were then single-cell cloned on 96-well plates to create clones with distinct levels of expression.

T-cell functional assays

Cytokine release was assayed by coincubating 1×10^5 CAR^+ T cells with 1×10^5 tumor cell targets in complete RPMI1640. At 24 hours, culture media were collected and cytokines were measured by a Human Proinflammatory Panel V-plex Human Tissue Culture multiplex

assay (Meso Scale Discovery). In some experiments, IL2 and IFNγ were measured by ELISA (BioLegend). Killing assays were performed by coculturing 5×10^4 CAR^+ T cells with 5×10^4 GFP-positive tumor cell targets in complete RPMI1640 in a 96-well plate and acquiring images every 2–3 hours using an Incucyte (Sartorius). Percent tumor cells remaining were calculated by dividing the total green fluorescence intensity at every time point by the same measurement at the first time point. CD69 and CD107a assays were performed by coculturing 1×10^5 CAR^+ T cells with 1×10^5 tumor cell targets in complete RPMI1640 in the presence of monensin and CD107a antibody (BioLegend, clone H4A3, BV605). After 6 hours, cells were harvested, washed, and then stained with Fixable viability dye (eBioscience, eFluor 780), huCD45 (eBioscience, clone HI30, PerCP-Cyanine5.5), and CD69 (BioLegend, clone FN50, BV421). Cells were gated on viable single cells that were GFP^- (tumor cells expressed GFP) and $huCD45^+$ to assess both the % CD69- and/or CD107a-positive cells and the mean fluorescence intensity for both CD69 and CD107a. To determine B7-H3 expression on tumor cells after exposure to B7-H3 CAR T cells, 1×10^5 CAR^+ T cells or MOCK untransduced T cells were cocultured with 1×10^5 tumor cell targets in complete RPMI1640 for 80 hours. After 80 hours, cells were analyzed by flow cytometry for B7-H3 expression.

Assessment of secreted soluble B7-H3

A total of 1×10^5 tumor cells were plated in triplicate for 24 hours in 200 μL of complete RPMI1640. Supernatant was collected and then used in a Human B7-H3 Quantikine ELISA Kit (R&D Systems).

Antibodies and flow cytometry analyses

Staining for B7-H3 expression on tumor lines was performed with phycoerythrin (PE)- or APC-conjugated mouse anti-human B7-H3 antibody (R&D Systems, clone MAB1027). B7-H3 surface molecule number was calculated the Quantibrite Kit (BD Biosciences) according to the manufacturer's protocol. CAR expression on transduced T cells was also measured by flow cytometry. CAR T cells were stained with Biotin-Protein L (Thermo Fisher Scientific), followed by fluorophore-conjugated streptavidin (BD Biosciences). All staining was performed in 0.1-mL FACS buffer (PBS + 2% BSA). Flow cytometry was performed using a FACS Fortessa (BD Biosciences) and analyzed with FlowJo software (Tree Star). For the T-cell exhaustion and phenotyping panel, T cells were stained with anti-human LAG-3 (eBioscience, clone 3DS223H, PE), PD-1 (eBioscience, clone J105, PE-Cy7), TIM3 (BioLegend, clone F38–2E2, BV510), CD4 (BD Biosciences, clone SK3, BUV395), and CD8 (BD Biosciences, clone SK1, BUV805). Cell phenotype of monocytes was confirmed by staining for CD11b (BD Biosciences, clone ICRF44, PE-Cy7) and CD14 (BD Biosciences, clone M5E2, BV605) and of monocyte-derived dendritic cells (moDC) by staining for CD-80 (BioLegend, clone 2D10, BV605), HLA-DR (BioLegend, clone L243, BV421), and CD11c (BioLegend, clone Bu15, PE-Cy7).

Mice

Immunodeficient NSG mice (NOD.Cg-Prkdcscid Il2rgtm1Wjl/SzJ) were purchased from The Jackson Laboratory or bred in house. Mice used for *in vivo* experiments were between 6 and 12 weeks old and the ratio of male to female mice was matched in experimental

and control groups. All animal studies were carried out according to NCI and Stanford University Animal Care and Use Committee–approved protocols.

MG63.3 osteosarcoma *in vivo* models

Animal studies were carried out under protocols approved by the NCI Bethesda and Stanford University Animal Care and Use Committees. Cell lines were expanded under standard culture conditions (described above) and harvested with 2 mmol/L EDTA (KD Medical) in PBS (Gibco, Thermo Fisher Scientific) or Trypsin (Gibco, Thermo Fisher Scientific). For MG63.3, 1e6 cells were injected periostal to the tibia. In the direct tumor shrinkage experiments, 1e7 B7-H3 CAR^+ T cells or an equivalent number of CD19 CAR T cells (matched for total T-cell dose) were injected intravenously into a tail vein 2–3 weeks after tumor inoculation (once the majority of tumors had an area greater than 75 mm^2). Tumor growth was measured with digital calipers once to twice weekly, and the tumor area was calculated by multiplying the lengths of the major and minor axes. Mice were euthanized when the tumor exceeded a size set by institutional protocol. In the metastatic model experiments, once the bulk of the mouse tumors reached greater than 12.5 mm in one direction, the tumor-bearing leg of all mice was amputated using sterile technique under isoflurane anesthesia. Buprenorphine 0.05 mg/kg was injected subcutaneously for pain control. Mice were randomized to B7-H3 CAR treatment or no treatment groups based on their preamputation tumor sizes and groups were statistically identical. Five days after amputation, experimental mice were treated with 1e7 B7-H3 CAR^+ T cells.

EW8 Ewing sarcoma *in vivo* models

2e6 EW8 cells were injected periosteal to the tibia. 1e7 B7-H3 CAR^+ T cells or an equivalent number of CD19 CAR T cells (matched for total T-cell dose) were injected intravenously into a tail vein 2 weeks after tumor inoculation. Tumor growth was measured with digital calipers once to twice weekly, and the tumor area was calculated by multiplying the length of the major and minor axes. Mice were euthanized when the tumor exceeded a size set by the institutional protocol.

DAOY medulloblastoma *in vivo* models

As described previously (37), mice were anesthetized with 50 mg/kg ketamine and 0.5 mg/kg dexmedetomidine by intraperitoneal (i.p.) injection. The mice were immobilized in a mouse stereotaxic device (Stoelting). The head was shaved and scrubbed with 1% povidone-iodine, then a 1-cm skin incision was made along the midline and a burr hole was made using an 18G needle 2 mm anterior and 1 mm to the right of the lambda. Using a 28G needle mounted on a Hamilton syringe, 5e4 GFP-luciferase–expressing DAOY cells in 5 μL were injected 3-mm deep from the surface of the skull over 5 minutes. The needle was slowly retracted and the incision closed using wound clips. Mice were treated with 1 mg/kg atipamezole i.p. to reverse the effects of dexmedetomidine. Buprenorphine 0.05 mg/kg was injected subcutaneously for pain control. Seven to 10 days after tumor implantation and after confirmation of tumor formation by bioluminescence, mice were treated with 1e7 B7-H3 CAR^+ T cells or an equivalent number of CD19 CAR T cells (matched for total T-cell dose) intravenously by tail vein injection. Isoflurane-anesthetized animals were imaged using the IVIS system (Caliper Life Science) 10 minutes after 3 mg D-luciferin (PerkinElmer)

was injected intraperitoneally. Living Image (Caliper Life Sciences) software was used to analyze the IVIS data. Animals were imaged initially to confirm tumor implantation and then imaged twice weekly.

D425 medulloblastoma *in vivo* models

As described previously (38), mice were anesthetized with 3% isoflurane (Minrad International) in an induction chamber. Anesthesia on the stereotactic frame (David Kopf Instruments) was maintained at 2% isoflurane delivered through a nose adaptor. D425 medulloblastoma cells were injected at coordinates 2 mm posterior to lambda on midline and 2 mm deep into 6- to 10-week-old NOD-SCID gamma mice using a blunt-ended needle (75N, 26s/2″/2, 5 μL; Hamilton Co.). Using a microinjection pump (UMP-3; World Precision Instruments), 2e4 D425-GFP-Luc cells were injected in a volume of 3 μL at 30 nL/s. After leaving the needle in place for 1 minute, it was retracted at 3 mm/min. Tumor formation was followed by bioluminescence imaging on an IVIS spectrum instrument (Caliper Life Science) in the Stanford Small Animal Imaging Facility and quantified with Living Image software (PerkinElmer). Four days after tumor implantation and after confirmation of tumor formation by bioluminescence, mice were randomized and treated with 1e7 B7-H3 CAR^+ T cells or an equivalent number of CD19 CAR T cells (matched for total T-cell dose) intravenously by tail vein injection. Isoflurane-anesthetized animals were imaged using the IVIS system (Caliper Life Sciences) 10 minutes after 3 mg D-luciferin (PerkinElmer) was injected intraperitoneally. Living Image (PerkinElmer) software was used to analyze the IVIS data.

Immunofluorescence in D425 models

Mice were deeply anesthetized with tribromoethanol (Avertin) before being perfused transcardially with cold PBS (2 mice per group at two time points, day +7 and day +12 after CAR T-cell infusion). Brains were fixed overnight in 4% PFA/PBS and transferred to 30% sucrose for 2 days. Serial 40-μmcoronal sections were then cut on a freezing microtome. Serially sampled sections (1:12 series) were sampled and counterstained with DAPI. Mounted samples were imaged by confocal microscopy (Zeiss LSM710), and acquired Z stacks were flattened by maximum intensity projection (ImageJ). Tile images were acquired on an upright epifluorescence microscope with motorized stage (Zeiss AxioImager M2) and tile scanning software (MBF Bioscience).

K562 and NALM6 Leukemia *in vivo* models

For K562, 1.5e6 tumor cells were transferred to NSG mice by tail vein injection. Five days later, 1e7 B7-H3 CAR^+ T cells or an equivalent total number of mock/untransduced T cells were transferred intravenously. For NALM6-GL-B7-H3, 1e6 tumor cells were transferred to NSG mice by tail vein injection. Three to five days later, 1e7 B7-H3 CAR^+ T cells or an equivalent total number of mock/untransduced T cells were transferred intravenously. NALM6-GL leukemia burden was evaluated using the Xenogen IVIS Lumina (Caliper Life Sciences). Mice were injected intraperitoneally with 3 mg D-luciferin (PerkinElmer) and then imaged 4 minutes later with an exposure time of 30 seconds. Luminescence images were analyzed using Living Image software (PerkinElmer).

Confirmation of antigen expression of tumor cell lines *in vivo*

Indicated cell lines were engrafted into a mouse as was performed in the therapeutic experiments. Tumors were allowed to grow until mice became morbid and then were harvested (K562 from liver; NALM6-B7-H3 lines from bone marrow; EW8 and MG63.3 from orthotopic solid tumors). Single-cell suspensions were made from tumor samples and red blood cells were lysed with ACK lysis buffer. Cell suspensions were stained for B7-H3 (R&D Systems, clone MAB1027, APC) alongside cell lines with a fixable viability dye (eBioscience, eFluor 780). Tumor cells were gated by GFP except in the case of EW8 in which cells were also stained for human HLA-ABC (BD Biosciences, clone G46-2.6, FITC) and K562 in which cells were also stained for human CD45 (BioLegend, clone HI30, PE).

Monocyte and dendritic cell acquisition

PBMCs were isolated from peripheral blood of healthy donors by Ficoll-Paque PLUS (GE Healthcare) gradient centrifugation. T cells were purified using the EasySep Human CD3 Positive Selection Kit (StemCell Technologies). Monocytes were purified from the residual fraction of the same sample using the EasySep Human CD14 Positive Selection Kit II (StemCell Technologies) and were cultured at 1×10^6 cells/mL in RPMI containing 10% FBS supplemented with 1,000 U/mL human recombinant GM-CSF (PeproTech) and 500 U/mL human recombinant IL4 (PeproTech) to generate moDCs. MoDCs were cultured for 7 days with replacement of half of the culture volume with fresh media on days 3 and 5. CAR T cells were generated as described above from the same donors as the monocytes.

Graphs and statistical analysis

Data were visualized and analyzed using GraphPad Prism software. Graphs represent either group mean values ± SEM or individual values. All inset graphs are the averages of individual values seen. The *P* values were calculated with log-rank statistics for survival analyses, the repeated-measures ANOVA for tumor growth curves, and Student *t* tests for *in vitro* cytokine data and ANOVA for CD69/CD107a expression. $P < 0.05$ was considered statistically significant, and *P* values are denoted with asterisks as follows: $P > 0.05$; not significant, NS; *, $P < 0.05$; **, $P < 0.01$; ***, $P < 0.001$; and ****, $P < 0.0001$.

Results

B7-H3 is highly and homogenously expressed on pediatric solid tumors

Tumor microarrays (TMA) were stained by IHC for expression of B7-H3. Of 388 tumor samples, comprising pediatric solid tumors and brain tumors, 325 (84%) were positive for B7-H3, with 70% demonstrating high intensity staining of 2+ or 3+. Representative images are shown in Fig. 1A. Expression was typically homogeneous, with 291 (90%) of the positive samples staining positive for B7-Hy3 in 100% of the tumor cells on the core. A complete description of the IHC results is provided in Table 1. Greater than 90% of pediatric sarcomas tested expressed B7-H3, with rhabdomyosarcoma (alveolar and embryonal) and Ewing sarcoma samples demonstrating consistently high staining intensities and H-scores, defined as the product of staining intensity and % of stained cells (Fig. 1B; Table 1). B7-H3 was also highly expressed in Wilms tumor and neuroblastoma (Fig. 1C).

Ganglioneuroblastoma and ganglioneuroma, more differentiated forms of neuroblastoma, demonstrated lower intensity staining and less frequent expression (Fig. 1C). Pediatric brain tumors were also analyzed, including medulloblastoma, high-grade gliomas (anaplastic astrocytoma and glioblastoma multiforme), and diffuse intrinsic pontine glioma (DIPG, recently reclassified by WHO as diffuse midline glioma, H3K27M mutant). Again, the majority of samples were positive, including 100% of the DIPG samples, albeit with lower mean intensity than the other two CNS tumor types (Fig. 1D).

Derivation of a novel B7-H3 CAR

Given the promising high and homogeneous expression of B7-H3 on pediatric tumor tissues, we generated B7-H3 directed CAR T cells. Six anti-B7-H3 CARs were initially generated. Five fully human scFvs (CD276.1, CD276.2, CD276.3, CD276.4, and CD276.5) were obtained by screening a yeast display library and a sixth humanized scFv (CD276.MG) was obtained as a collaboration with MacroGenics. Of note, the scFv from MacroGenics contains the same DNA sequence found in enoblituzumab (MGA271), a humanized antibody that recognizes an epitope of B7-H3 with high tumor reactivity and restricted expression on normal human tissues (30). Second-generation CARs with a 4-1BB costimulatory domain and a short hinge region were generated (Supplementary Fig. S1A). Using a gamma retrovirus, the CARs were expressed on primary T cells (Supplementary Fig. S1B) and screened for antigen-induced IFNγ production. Two of the six constructs, CD276.MG-4–1BB-ζ and CD276.3-4-1BB-ζ, showed superior function against cell lines expressing B7-H3 and were thus selected for further study (Supplementary Fig. S1C). The CARs that expressed at lower levels on the surface of T cells (CD276.1, CD276.2, and CD276.5) did not produce significant amounts of IFNγ (Supplementary Fig. S1B and S1C), in line with our previously published work demonstrating that adequate surface CAR expression is required for efficacy (18). To determine whether other CAR structures could impart superior functionality, the CARs were reengineered to contain either an extracellular spacer domain (CH2-CH3 from IgG1, Supplementary Fig. S1D) or an additional costimulatory domain (CD28–41BB-ζ, third-generation CAR, Supplementary Fig. S1E). After coculture with B7-H3-expressing cell lines, we found that these reengineered CARs produced less cytokine than the original CARs with 4-1BB costimulatory domains (Supplementary Fig. S1F). In addition, we found that the MGA271-based CAR, CD276.MG-4-1BB-ζ, here-after referred to as the B7-H3 CAR, produced the most cytokine in response to tumor and thus it was chosen for further testing both *in vitro* and *in vivo*.

We previously demonstrated that tonic signaling can drive T-cell exhaustion and contributes to failure of certain CAR constructs (39). To test whether the B7-H3 CAR was superior to CD276.3 due to T-cell exhaustion, we evaluated CARs transduced with each construct for the expression of exhaustion markers PD-1, TIM-3, and LAG3, but we did not see major differences between the two that could account for their differential activity (Supplementary Fig. S1G). CD4 versus CD8 ratios for the B7-H3 CAR versus untransduced (MOCK) T cells are shown in Supplementary Fig. S1H.

B7-H3 CAR T cells eradicate osteosarcoma and Ewing sarcoma xenografts *in vivo*

We first tested the B7-H3 CAR *in vivo* against MG63.3, a xenograft model of osteosarcoma with strong metastatic potential (40). When cocultured with this tumor line, B7-H3 CAR T cells specifically produced IFNγ, TNFα, and IL2 (Fig. 2A). NSG mice were orthotopically injected with 1e6 MG63.3 cells in the hind leg. Two to three weeks later, when all or most of the mice had measurable tumor with an area greater than 75 mm^2, animals received 1e7 intravenously administered B7-H3 CAR T cells or negative control CD19 CAR T cells (CD19 is not expressed by these solid tumors; Fig. 2B). The B7-H3 CAR T cells mediated complete regression and eradication of xenografts (Fig. 2C), leading to a significant survival advantage compared with control CAR T-cell–treated mice (Fig. 2D).

We also took advantage of the metastatic potential of this aggressive tumor line to evaluate the potential for B7-H3 CAR T cells to mediate activity against metastatic disease (Fig. 2E). MG63.3 was clonally derived from the MG63 cell line because of its propensity to metastasize to the lungs (40). Mice were orthotopically injected with 1e6 MG63.3 tumor cells in the hind limb. Tumors were allowed to grow until they were approximately 12.5 mm in the longest dimension, at which point the hind leg and tumor were amputated. Five days later, mice were treated with 1e7 B7-H3 CAR T cells (Fig. 2E). Because irrelevant CD19 control or mock-transduced T cells cause xenogeneic graft versus host disease (GVHD) and complicate long-term survival analysis, we compared B7-H3 CAR T cells to no treatment in this metastatic model (discussed below). All untreated mice died within 50 days of amputation, whereas 9 of 10 mice who received B7-H3 CAR T cells survived longer than 5 months (Fig. 2F). At the time of death for the control mice, lungs of some mice were harvested to confirm the presence of metastasis, which could be grossly seen replacing most of the lung tissue. Therefore, B7-H3 CAR T cells mediate activity against both established and metastatic osteosarcoma xenografts.

To confirm activity in an additional model of pediatric sarcomas, we elected to test the B7-H3 CAR against a Ewing sarcoma xenograft. Two weeks after orthotopic tumor inoculation of 2e6 EW8 cells in the hind limb, NSG mice were treated with 1e7 intravenously administered B7-H3 CAR T cells or control CD19 CAR T cells (Fig. 3A). The B7-H3 CAR T cells eradicated tumor (Fig. 3B), leading to a significant survival advantage compared with control-treated mice (Fig. 3C).

B7-H3 CAR T cells mediate activity against pediatric CNS tumors

When cocultured with medulloblastoma cell lines or DIPG patient–derived cultures (34), B7-H3 CAR T cells specifically produced IFNγ, TNFα, and IL2 (Fig. 4A). To test whether the B7-H3 CAR can effectively cross the blood–brain barrier and eradicate CNS tumors, we intravenously administered 1e7 B7-H3 CAR T cells to mice bearing DAOY medulloblastoma xenografts (engineered to express GFP luciferase) in the posterior fossa (Fig. 4B). B7-H3 CAR T cells eradicated the autochthonous xenografts as measured by bioluminescent imaging (BLI, Fig. 4C and D). We then tested the CAR against a more aggressive c-MYC–amplified group 3 medulloblastoma xenograft, D425, which often metastasizes to the leptomeninges and spinal cord (ref. 41; Fig. 4E). Again, intravenously administered B7-H3 CAR T cells cleared the disease by BLI (in 4 of 6 mice; Fig. 4F and

G), leading to significantly prolonged survival (Fig. 4H). To better illustrate CAR T-cell trafficking to the CNS, we fused both the B7-H3 CAR and the CD19 CAR to the fluorescent protein mCherry and visualized mouse cerebellum at two time points after treatment in the D425 model by confocal microscopy. Confocal microscopy demonstrates that B7-H3 CAR T cells enter the CNS within 7 days of treatment to eradicate tumor cells while control CAR T cells are not found in significant numbers in the CNS (Fig. 4I).

B7-H3 CAR T cells demonstrate a therapeutic window that can be exploited

B7-H3 expression has previously been reported on lymphoid and myeloid leukemias (42). K562, an erythromyeloid leukemia, expresses B7-H3. We intravenously injected NSG mice with 1.5e6 K562 cells and then treated the mice with 1e7 B7-H3 CAR or MOCK untransduced T cells 5 days later (Fig. 5A). Although the B7-H3 CAR demonstrated activity and prolonged survival in this model (Fig. 5B), the results were not as striking as in our models of sarcoma and medulloblastoma, which was surprising given the clinical success of CARs in hematologic malignancies versus solid tumors. We ruled out the possibility that some of our tumor cells could be secreting B7-H3 that inhibits CAR activity as we did not detect B7-H3 protein in supernatant from tumor cells by ELISA (Supplementary Fig. S2A). We also confirmed that B7-H3 expression was maintained on all cell lines engrafted into mice at similar levels to expression on the cell line in culture (Supplementary Fig. S2B). We hypothesized that the limited activity of the B7-H3 CAR in this model was due to lower expression of B7-H3 on K562 than the other cell lines against which the CAR demonstrated impressive activity (Fig. 5C and D).

To test this hypothesis, we lentivirally expressed B7-H3 on the surface of NALM6, a B-cell leukemia known to be susceptible to CAR T cells and obtained single clones expressing variable amounts of B7-H3 on their surface (Fig. 6A and B). CAR T cells were tested in *in vitro* assays against NALM6 lines expressing variable amounts of B7-H3. Both, tumor cell killing (Fig. 6C) as well as CD69 (T-cell activation) and CD107a (T-cell degranulation) expression by T cells in response to tumor encounter (Fig. 6D) were proportional to B7-H3 density on the tumor cells. Importantly, we detected minimal killing or T-cell activation when tumor cells expressed low levels of B7-H3. There was no significant increase in the production of inflammatory cytokines by B7-H3 CAR T cells against low B7-H3–expressing NALM6 as compared with the B7-H3–negative NALM6 wild-type line. However, the B7-H3 CAR produced cytokines in response to NALM6 cells expressing greater amounts of B7-H3 (Fig. 6E and F).

NSG mice were then inoculated with 1e6 NALM6 cells expressing either low or medium amounts of B7-H3 and then treated with B7-H3 CAR T cells or control untransduced MOCK CAR T cells (Fig. 6G). When leukemia cells expressed adequate B7-H3, the B7-H3 CAR mediated disease control (Fig. 6H and J). However, when NALM6 cells expressed lower levels of B7-H3, the CAR T cells demonstrated minimal *in vivo* activity (Fig. 6I and K). Of note, no additional *in vivo* activity was seen when treating mice with leukemia expressing even higher levels of B7-H3 (Supplementary Fig. S3).

To confirm that antigen loss did not account for these findings, we assessed B7-H3 expression on tumor cells after an 80-hour period of coculture with B7-H3 or MOCK CAR

T cells (Supplementary Fig. S2C). Antigen downregulation was not observed. We conclude therefore that the differences in tumor cell killing and *in vivo* activity are due to differences in antigen-driven T-cell activation and proliferation. In summary, B7-H3 CAR T cells are promising for tumors with high-level antigen expression and data are consistent with a therapeutic window in which low-level expression on normal tissue may not elicit toxicity.

Discussion

We present here preclinical results using a novel CAR targeting B7-H3, a pan-cancer antigen broadly expressed on many pediatric solid tumors. In addition, we present the largest screen to date of pediatric tumor tissues for the expression of B7-H3. This molecule is highly and homogeneously expressed on numerous, common pediatric solid tumors, such as Ewing sarcoma, rhabdomyosarcoma, Wilms tumor, neuroblastoma, as well as CNS malignancies such as medulloblastoma. Homogeneous antigen expression is important for CAR T-cell–based therapies as tumor target heterogeneity is a limiting factor in treating malignancies with these powerful yet specific therapeutics (43, 44), and the relatively low mutational burden in these cancers is expected to limit the degree of epitope spreading induced by CAR T cells (21). Other groups have similarly demonstrated expression of B7-H3 on DIPG (24), osteosarcoma (23), and neuroblastoma (45). The prognosis of the diseases tested here following relapse remains poor and this novel CAR could present a new therapeutic option. In addition, we demonstrate expression on DIPG and high-grade gliomas, although *in vivo* efficacy remains to be tested in pediatric gliomas.

The exact function of this molecule is unclear, as its ligand(s) remain unknown. It was initially thought to be involved in T-cell costimulation (46, 47); however, there is substantial evidence for a model wherein B7-H3 mediates an immune-suppressive, check-point-like role (48, 49). It has long been recognized as a potential target in cancer for antibody therapy (45) and, more recently, preclinical studies of an antibody–drug conjugate, which targets both the tumor itself and tumor vasculature, were published (35).

Despite initially drawing on a large yeast display Fab library to identify possible binders, ultimately our most efficacious CAR incorporated a binder from a previously published antibody (30). Although we have previously used a similar Fab library to generate a highly active CAR against CD22 that is currently in clinical trials (50), this work serves as a reminder that antibodies that are readily available can be used to generate highly active CARs. Indeed, almost all versions of the CD19 CAR in clinical trials are based on previously described murine antibodies (51, 52). Some of the differences in CAR efficacy between our binders appear to be related to lower CAR expression, which we previously reported can significantly impact CAR T-cell function (18).

Our B7-H3 CAR based on MGA271 demonstrated impressive *in vivo* activity against pediatric bone sarcomas as well as medulloblastoma. Systemic administration of B7-H3 CAR T cells mediated regression and eradication of established osteosarcoma and Ewing sarcoma xenografts, whereas no significant tumor control was observed with mock-transduced cells. In addition, drawing on a highly metastatic model of osteosarcoma with 100% lethality (40), we demonstrate near complete survival after treatment with the B7-H3

CAR, introducing the possibility that it could eventually be applied in an adjuvant setting for patients with high-risk disease following standard therapy. Our metastatic model is limited by an inability to give mock T cells due to the universal development of lethal xenogeneic GVHD in mice given irrelevant or untransduced CAR T cells. However, the localized MG63.3 experiment demonstrates that the B7-H3 CAR antitumor effect is not xenogeneic. In addition, administering unmanipulated naïve T cells has previously been shown to prevent osteosarcoma metastases in a murine model (50). However, this finding is unlikely to be clinically relevant given the failure of allogeneic stem cell transplantation to improve outcomes for children with solid tumors (51), while the B7-H3 CAR represents a novel, directly targeted approach that does not rely on GVHD for antitumor effect.

The B7-H3 CAR also mediates complete regression and clearance of two autochronous medulloblastoma xenografts (D425 and DAOY) when delivered intravenously. In a recent case report, intrathecally delivered CAR T cells mediated regression in an adult patient with glioblastoma multiforme (53), raising hopes that patients may be able to be treated with CAR T cells delivered regionally, potentially avoiding systemic toxicity. Whether local delivery would be more effective than systemic delivery utilized here is an area of ongoing study.

Activity against K562, a xenograft erythromyeloid leukemia line, was more modest. While B7-H3 CAR T cells significantly extended survival compared with mice treated with untransduced T cells, the response was not universal or prolonged. We hypothesize that the activity of the CAR in this model is limited by lower B7-H3 antigen density on hematologic malignancies. Indeed, when we overexpressed the antigen on the NALM6 B-cell leukemia line at higher levels, the CAR mediated *in vivo* activity. But when we expressed lower levels of the antigen on the same cell line, the CAR demonstrated minimal activity, indicating that a threshold of antigen density is required to mediate *in vivo* activity. This disparity in *in vivo* functionality is supported by differences in antigen-driven T-cell activation and degranulation, tumor cell killing, and T-cell cytokine production. We and others have previously demonstrated the importance of antigen density to CAR functionality (18–20, 50).

For the B7-H3 CAR, a window in which some expression of the antigen on normal tissue may be below the threshold required for CAR efficacy could represent an advantage for targeting this pan-cancer antigen that is expressed at lower levels on normal tissue. Furthermore, while B7-H3 is expressed on some normal tissues, the antibody on which this CAR is based (MGA271) demonstrates minimal binding to normal tissues, as previously published in this journal by Loo and colleagues (30). MGA271 has been safely used in early-phase clinical trials without major toxicities and has resulted in clinically meaningful responses (31). A phase I trial in children is ongoing (NCT02982941) as are trials of this agent in combination with PD-1 inhibitors (NCT02475213). A CD3 × B7-H3 bispecific molecule that uses this same binder is in clinical trials in adults as well (NCT02628535). 8H9, another antibody targeting B7-H3, has also been safely used in clinical trials as a radioconjugate administered directly into the CNS of pediatric patients for more than 10 years (29, 54) and has more recently shown clinical promise when directly administered into the abdomen of patients with desmoplastic small round cell tumor (33).

Of interest, previous work has shown that B7-H3 expression can be induced on normal tissue in response to inflammation (48), and safety of this novel therapeutic can only be accurately assessed in the context of a carefully designed clinical trial. Interestingly, when we differentiated monocytes to dendritic cells *in vitro* by culturing them in IL4 and GM-CSF, we observed significant levels of B7-H3 expression and CAR reactivity (Supplementary Fig. S4). The level of B7-H3 on human dendritic cells *in vivo* has not been assessed and the clinical effects of CAR-mediated targeting of dendritic cells are unknown. If toxicity is observed, logic-gated CAR T cells (55) and/or probodies that mask a CAR except when the T cell is within the tumor microenvironment (56) could be developed to allow targeting of this broadly expressed tumor-associated molecule.

In summary, we report on a CAR T cell directed at B7-H3 that shows strong activity against a wide array of xenograft pediatric cancer models including solid, liquid, and CNS tumors. We demonstrate that CAR T-cell activity is dependent on antigen density, as has emerged for many CAR therapeutics. This CAR may provide a new therapeutic option for children with incurable, metastatic, or chemo-refractory disease and should be carefully studied in early-phase clinical trials.

Supplementary Material

Refer to Web version on PubMed Central for supplementary material.

Acknowledgments

The authors would like to thank John Buckley for his technical assistance. This research was supported by the Intramural Research Program of the NIH, CCR, NCI. R.G. Majzner is supported by a Sarcoma Alliance for Research Through Collaboration (SARC) Career Development Award, the Be Brooks Brave Fund St. Baldrick's Scholar Award, and a Hyundai Hope on Wheels Young Investigator Award. This research was also supported by the St. Baldrick's-Stand Up to Cancer Dream Team Translational Research Grant (SU2C-AACR-DT-27-17). Stand Up to Cancer is a division of the Entertainment Industry Foundation. Research Grants are administered by the American Association for Cancer Research, the Scientific Partner of SU2C. C.L.M. is a member of the Parker Institute for Cancer Immunotherapy, which supports the Stanford University Cancer Immunotherapy Program. J.L. Theruvath is supported by German Cancer Aid (Deutsche Krebshilfe) grant P-91650709.

Disclosure of Potential Conflicts of Interest

C. Rota is an employee of Dana Farber Cancer Institute. D.W. Lee reports receiving commercial research grants from Kite Pharma and Gilead, and is a consultant/advisory board member for Juno Therapeutics and Celgene. R.J. Orentas is a consultant/advisory board member for Lentigen Technology and Otter Immuno-Oncology. E. Bonvini is an employee of and holds ownership interest (including patents) in MacroGenics. R. Majeti is an employee of, holds ownership interest (including patents) in, and is a consultant/advisory board member for Forty Seven Inc. J.M. Maris is a consultant/advisory board member for Lilly and Bayer. C.L. Mackall is an employee of Lyell Immunopharma; reports receiving commercial research grants from Bluebird Bio and Obsidian; holds ownership interest (including patents) in Lyell Immunopharma, Juno Therapeutics, and Allogene; and is a consultant/advisory board member for Unum Therapeutics, Glaxo-Smith Kline, Adaptimmune, Servier/Pfizer, Roche, Allogene, PACT Pharma, and Nektar. No potential conflicts of interest were disclosed by the other authors.

References

1. Smith MA, Altekruse SF, Adamson PC, Reaman GH, Seibel NL. Declining childhood and adolescent cancer mortality. Cancer2014;120:2497–506. [PubMed: 24853691]
2. Perkins SM, Shinohara ET, DeWees T, Frangoul H. Outcome for children with metastatic solid tumors over the last four decades. PLoS One2014;9: e100396. [PubMed: 25003594]

3. Packer RJ. Childhood brain tumors: accomplishments and ongoing challenges. J Child Neurol2008;23:1122–7. [PubMed: 18952578]
4. Rodriguez-Galindo C, Billups CA, Kun LE, Rao BN, Pratt CB, Merchant TE, et al.Survival after recurrence of Ewing tumors: the St Jude Children's Research Hospital experience, 1979–1999. Cancer2002;94:561–9. [PubMed: 11900241]
5. Tomlinson FH, Scheithauer BW, Meyer FB, Smithson WA, Shaw EG, Miller GM, et al.Medulloblastoma: I. Clinical, diagnostic, and therapeutic overview. J Child Neurol1992;7:142–55. [PubMed: 1573231]
6. Ebb D, Meyers P, Grier H, Bernstein M, Gorlick R, Lipshultz SE, et al.Phase II trial of trastuzumab in combination with cytotoxic chemotherapy for treatment of metastatic osteosarcoma with human epidermal growth factor receptor 2 overexpression: a report from the Children's Oncology Group. J Clin Oncol2012;30:2545–51. [PubMed: 22665540]
7. Pappo AS, Vassal G, Crowley JJ, Bolejack V, Hogendoorn PC, Chugh R, et al.A phase 2 trial of R1507, a monoclonal antibody to the insulin-like growth factor-1 receptor (IGF-1R), in patients with recurrent or refractory rhabdomyosarcoma, osteosarcoma, synovial sarcoma, and other soft tissue sarcomas: results of a Sarcoma Alliance for Research Through Collaboration study. Cancer2014;120:2448–56. [PubMed: 24797726]
8. Postow MA, Chesney J, Pavlick AC, Robert C, Grossmann K, McDermott D, et al.Nivolumab and ipilimumab versus ipilimumab in untreated melanoma. N Engl J Med2015;372:2006–17. [PubMed: 25891304]
9. Davis KL, Fox E, Reid JM, Liu X, Minard CG, Weigel B, et al.ADVL1412: Initial results of a phase I/II study of nivolumab and ipilimumab in pediatric patients with relapsed/refractory solid tumors—A COG study. J Clin Oncol2017;35(15_suppl):10526.
10. Majzner RG, Heitzeneder S, Mackall CL. Harnessing the immunotherapy revolution for the treatment of childhood cancers. Cancer Cell2017;31: 476–85. [PubMed: 28366678]
11. Majzner RG, Simon JS, Grosso JF, Martinez D, Pawel BR, Santi M, et al.Assessment of programmed death-ligand 1 expression and tumor-associated immune cells in pediatric cancer tissues. Cancer2017;123: 3807–15. [PubMed: 28608950]
12. Mackall CL, Merchant MS, Fry TJ. Immune-based therapies for childhood cancer. Nat Rev Clin Oncol2014;11:693–703. [PubMed: 25348789]
13. Lee DW, Kochenderfer JN, Stetler-Stevenson M, Cui YK, Delbrook C, Feldman SA, et al.T cells expressing CD19 chimeric antigen receptors for acute lymphoblastic leukaemia in children and young adults: a phase 1 dose-escalation trial. Lancet2015;385:517–28. [PubMed: 25319501]
14. Maude SL, Frey N, Shaw PA, Aplenc R, Barrett DM, Bunin NJ, et al.Chimeric antigen receptor T cells for sustained remissions in leukemia. N Engl J Med2014;371:1507–17. [PubMed: 25317870]
15. Gardner RA, Finney O, Annesley C, Brakke H, Summers C, Leger K, et al.Intent-to-treat leukemia remission by CD19 CAR T cells of defined formulation and dose in children and young adults. Blood2017;129: 3322–31. [PubMed: 28408462]
16. Ahmed N, Brawley VS, Hegde M, Robertson C, Ghazi A, Gerken C, et al.Human epidermal growth factor receptor 2 (HER2)-specific chimeric antigen receptor-modified T cells for the immunotherapy of HER2-positive sarcoma. J Clin Oncol2015;33:1688–96. [PubMed: 25800760]
17. Ahmed N, Brawley V, Hegde M, Bielamowicz K, Kalra M, Landi D, et al.HER2-specific chimeric antigen receptor-modified virus-specific T cells for progressive glioblastoma: a phase 1 dose-escalation trial. JAMA Oncol2017;3:1094–101. [PubMed: 28426845]
18. Walker AJ, Majzner RG, Zhang L, Wanhainen K, Long AH, Nguyen SM, et al.Tumor antigen and receptor densities regulate efficacy of a chimeric antigen receptor targeting anaplastic lymphoma kinase. Mol Ther2017;25: 2189–201. [PubMed: 28676342]
19. Caruso HG, Hurton LV, Najjar A, Rushworth D, Ang S, Olivares S, et al.Tuning sensitivity of CAR to EGFR density limits recognition of normal tissue while maintaining potent antitumor activity. Cancer Res2015;75: 3505–18. [PubMed: 26330164]
20. Liu X, Jiang S, Fang C, Yang S, Olalere D, Pequignot EC, et al.Affinity-tuned ErbB2 or EGFR chimeric antigen receptor T cells exhibit an increased therapeutic index against tumors in mice. Cancer Res2015; 75:3596–607. [PubMed: 26330166]

21. Majzner RG, Mackall CL. Tumor antigen escape from CAR T-cell therapy. Cancer Discov2018;8:1219–26. [PubMed: 30135176]
22. Maus MV, June CH. Making better chimeric antigen receptors for adoptive T-cell therapy. Clin Cancer Res2016;22:1875–84. [PubMed: 27084741]
23. Wang L, Zhang Q, Chen W, Shan B, Ding Y, Zhang G, et al.B7-H3 is overexpressed in patients suffering osteosarcoma and associated with tumor aggressiveness and metastasis. PLoS One2013;8:e70689. [PubMed: 23940627]
24. Zhou Z, Luther N, Ibrahim GM, Hawkins C, Vibhakar R, Handler MH, et al.B7-H3, a potential therapeutic target, is expressed in diffuse intrinsic pontine glioma. J Neurooncol2013;111:257–64. [PubMed: 23232807]
25. Modak S, Kramer K, Gultekin SH, Guo HF, Cheung NK. Monoclonal antibody 8H9 targets a novel cell surface antigen expressed by a wide spectrum of human solid tumors. Cancer Res2001;61:4048–54. [PubMed: 11358824]
26. Picarda E, Ohaegbulam KC, Zang X. Molecular pathways: targeting B7-H3 (CD276) for human cancer immunotherapy. Clin Cancer Res2016;22: 3425–31. [PubMed: 27208063]
27. Tekle C, Nygren MK, Chen YW, Dybsjord I, Nesland JM, Maelandsmo GM, et al.B7-H3 contributes to the metastatic capacity of melanoma cells by modulation of known metastasis-associated genes. Int J Cancer2012;130: 2282–90. [PubMed: 21671471]
28. Ye Z, Zheng Z, Li X, Zhu Y, Zhong Z, Peng L, et al.B7-H3 Overexpression predicts poor survival of cancer patients: a meta-analysis. Cell Physiol Biochem2016;39:1568–80. [PubMed: 27626927]
29. Kramer K, Kushner BH, Modak S, Pandit-Taskar N, Smith-Jones P, Zanzonico P, et al.Compartmental intrathecal radioimmunotherapy: results for treatment for metastatic CNS neuroblastoma. J Neurooncol2010;97: 409–18. [PubMed: 19890606]
30. Loo D, Alderson RF, Chen FZ, Huang L, Zhang W, Gorlatov S, et al.Development of an Fc-enhanced anti-B7-H3 monoclonal antibody with potent antitumor activity. Clin Cancer Res2012;18:3834–45. [PubMed: 22615450]
31. Powderly J, Cote G, Flaherty K, Szmulewitz RZ, Ribas A, Weber J, et al.Interim results of an ongoing phase I, dose escalation study of MGA271 (Fc-optimized humanized anti-B7-H3 monoclonal antibody) in patients with refractory B7-H3-expressing neoplasms or neoplasms whose vasculature expresses B7-H3. J Immunother Cancer2015;3 (Suppl 2):O8.
32. Souweidane MM, Kramer K, Pandit-Taskar N, Zhou Z, Haque S, Zanzonico P, et al.Convection-enhanced delivery for diffuse intrinsic pontine glioma: a single-centre, dose-escalation, phase 1 trial. Lancet Oncol2018;19: 1040–50. [PubMed: 29914796]
33. Modak S, Carrasquillo J, LaQuaglia M, Pat Z, Heaton T, Cheung N-K, et al.Intraperitoneal radioimmunotherapy for desmoplastic small round cell tumor: Results of a phase I study (NCT01099644). In: Proceedings of the American Association for Cancer Research Annual Meeting 2018; 2018 Apr 14–18; Chicago, IL. Philadelphia (PA): AACR; 2018. Abstract nr CT006.
34. Lin GL, Monje M. A protocol for rapid post-mortem cell culture of diffuse intrinsic pontine glioma (DIPG). J Vis Exp2017;121:55360.
35. Seaman S, Zhu Z, Saha S, Zhang XM, Yang MY, Hilton MB, et al.Eradication of tumors through simultaneous ablation of CD276/B7-H3-positive tumor cells and tumor vasculature. Cancer Cell2017;31:501–15. [PubMed: 28399408]
36. Mount CW, Majzner RG, Sundaresh S, Arnold EP, Kadapakkam M, Haile S, et al.Potent antitumor efficacy of anti-GD2 CAR T cells in H3-K27M(+) diffuse midline gliomas. Nat Med2018;24:572–9. [PubMed: 29662203]
37. Nellan A, Rota C, Majzner R, Lester-McCully CM, Griesinger AM, Mulcahy Levy JM, et al.Durable regression of medulloblastoma after regional and intravenous delivery of anti-HER2 chimeric antigen receptor T cells. J Immunother Cancer2018;6:30. [PubMed: 29712574]
38. Zhang M, Hutter G, Kahn SA, Azad TD, Gholamin S, Xu CY, et al.Anti-CD47 treatment stimulates phagocytosis of glioblastoma by M1 and M2 polarized macrophages and promotes M1 polarized macrophages *in vivo*. PLoS One2016;11:e0153550. [PubMed: 27092773]
39. Long AH, Haso WM, Shern JF, Wanhainen KM, Murgai M, Ingaramo M, et al.4–1BB costimulation ameliorates T cell exhaustion induced by tonic signaling of chimeric antigen receptors. Nat Med2015;21: 581–90. [PubMed: 25939063]

40. Ren L, Mendoza A, Zhu J, Briggs JW, Halsey C, Hong ES, et al.Characterization of the metastatic phenotype of a panel of established osteosarcoma cells. Oncotarget2015;6:29469–81. [PubMed: 26320182]
41. Gholamin S, Mitra SS, Feroze AH, Liu J, Kahn SA, Zhang M, et al.Disrupting the CD47-SIRPalpha anti-phagocytic axis by a humanized anti-CD47 antibody is an efficacious treatment for malignant pediatric brain tumors. Sci Transl Med2017315;9. pii: eaaf2968. doi: 10.1126/scitranslmed.aaf2968.
42. Guery T, Roumier C, Berthon C, Renneville A, Preudhomme C, Quesnel B. B7-H3 protein expression in acute myeloid leukemia. Cancer Med2015;4: 1879–83. [PubMed: 26376842]
43. Sotillo E, Barrett DM, Black KL, Bagashev A, Oldridge D, Wu G, et al.Convergence of acquired mutations and alternative splicing of CD19 enables resistance to CART-19 immunotherapy. Cancer Discov2015;5: 1282–95. [PubMed: 26516065]
44. O'Rourke DM, Nasrallah MP, Desai A, Melenhorst JJ, Mansfield K, Morrissette JJD, et al.A single dose of peripherally infused EGFRvIII-directed CAR T cells mediates antigen loss and induces adaptive resistance in patients with recurrent glioblastoma. Sci Transl Med2017;9.
45. Ahmed M, Cheng M, Zhao Q, Goldgur Y, Cheal SM, Guo HF, et al.Humanized affinity-matured monoclonal antibody 8H9 has potent antitumor activity and binds to FG loop of tumor antigen B7-H3. J Biol Chem2015;290:30018–29. [PubMed: 26487718]
46. Chapoval AI, Ni J, Lau JS, Wilcox RA, Flies DB, Liu D, et al.B7-H3: a costimulatory molecule for T cell activation and IFN-gamma production. Nat Immunol2001;2:269–74. [PubMed: 11224528]
47. Luo L, Chapoval AI, Flies DB, Zhu G, Hirano F, Wang S, et al.B7-H3 enhances tumor immunity *in vivo* by costimulating rapid clonal expansion of antigen-specific CD8+ cytolytic T cells. J Immunol2004;173: 5445–50. [PubMed: 15494491]
48. Veenstra RG, Flynn R, Kreymborg K, McDonald-Hyman C, Saha A, Taylor PA, et al.B7-H3 expression in donor T cells and host cells negatively regulates acute graft-versus-host disease lethality. Blood2015;125: 3335–46. [PubMed: 25814530]
49. Steinberger P, Majdic O, Derdak SV, Pfistershammer K, Kirchberger S, Klauser C, et al.Molecular characterization of human 4Ig-B7-H3, a member of the B7 family with four Ig-like domains. J Immunol2004;172:2352–9. [PubMed: 14764704]
50. Fry TJ, Shah NN, Orentas RJ, Stetler-Stevenson M, Yuan CM, Ramakrishna S, et al.CD22-targeted CAR T cells induce remission in B-ALL that is naive or resistant to CD19-targeted CAR immunotherapy. Nat Med2017;24:20–8. [PubMed: 29155426]
51. Kochenderfer JN, Feldman SA, Zhao Y, Xu H, Black MA, Morgan RA, et al.Construction and preclinical evaluation of an anti-CD19 chimeric antigen receptor. J Immunother2009;32:689–702. [PubMed: 19561539]
52. Brentjens RJ, Latouche JB, Santos E, Marti F, Gong MC, Lyddane C, et al.Eradication of systemic B-cell tumors by genetically targeted human T lymphocytes co-stimulated by CD80 and interleukin-15. Nat Med2003;9: 279–86. [PubMed: 12579196]
53. Brown CE, Alizadeh D, Starr R, Weng L, Wagner JR, Naranjo A, et al.Regression of glioblastoma after chimeric antigen receptor t-cell therapy. N Engl J Med2016;375:2561–9. [PubMed: 28029927]
54. Kramer K, Smith M, Souweidane MM. Safety profile of long-term intra-ventricular access devices in pediatric patients receiving radioimmunotherapy for central nervous system malignancies. Pediatr Blood Cancer2014; 61:1590–2. [PubMed: 24777835]
55. Roybal KT, Rupp LJ, Morsut L, Walker WJ, McNally KA, Park JS, et al.Precision tumor recognition by T cells with combinatorial antigen-sensing circuits. Cell2016;164:770–9. [PubMed: 26830879]
56. Polu KR, Lowman HB. Probody therapeutics for targeting antibodies to diseased tissue. Expert Opin Biol Ther2014;14:1049–53. [PubMed: 24845630]

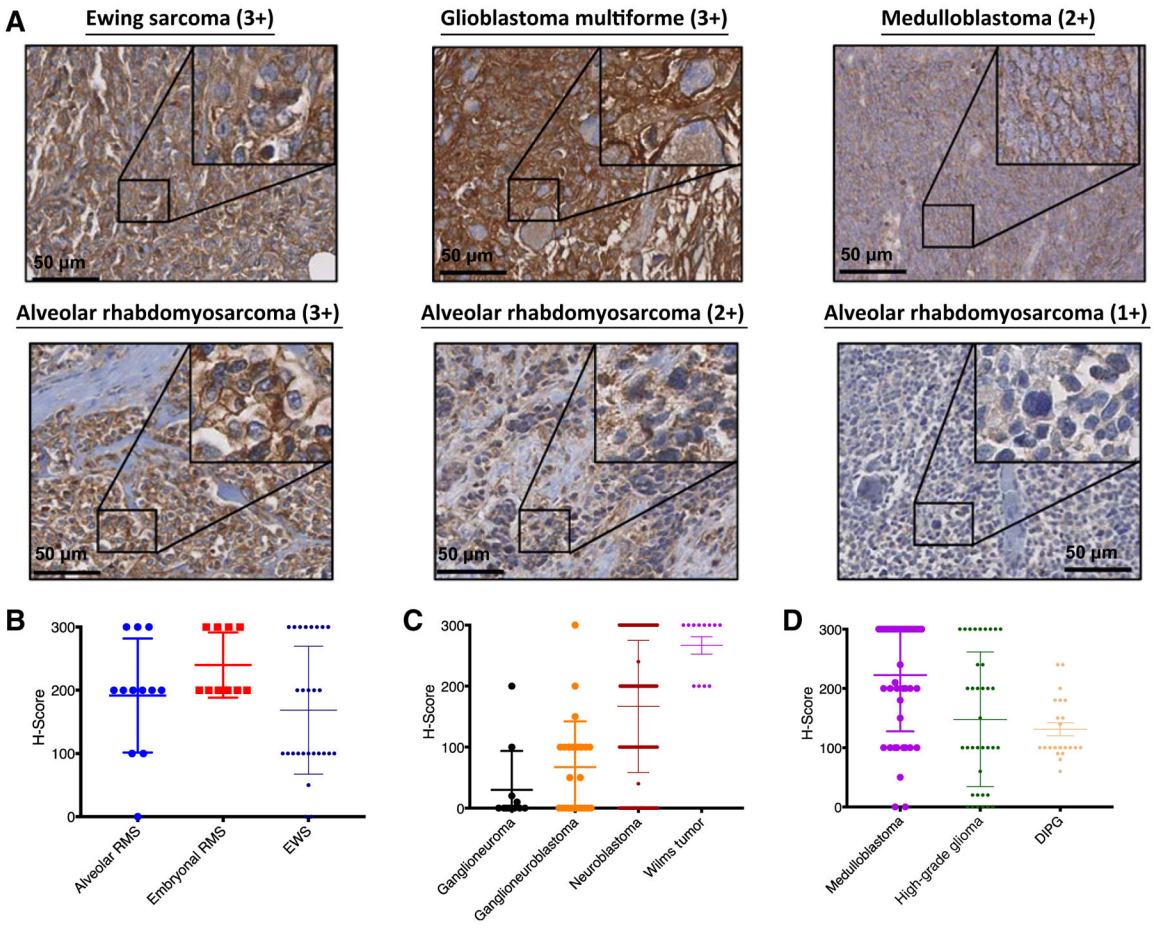

Figure 1.

B7-H3 is highly expressed on pediatric solid tumors. **A**, Pediatric tumor microarrays were stained by IHC for the expression of B7-H3. Representative images of Ewing sarcoma (3+), glioblastoma multiforme (3+), medulloblastoma (2+), and alveolar rhabdomyosarcoma (3+, 2+, and 1+) samples are shown. H-scores were generated by multiplying the % cells positive × intensity seen for each core. H-scores are shown for pediatric sarcomas (**B**), neuroblastoma and Wilms tumor (**C**), and pediatric CNS tumors (**D**). RMS, rhabdomyosarcoma; EWS, Ewing sarcoma; DIPG, diffuse intrinsic pontine glioma.

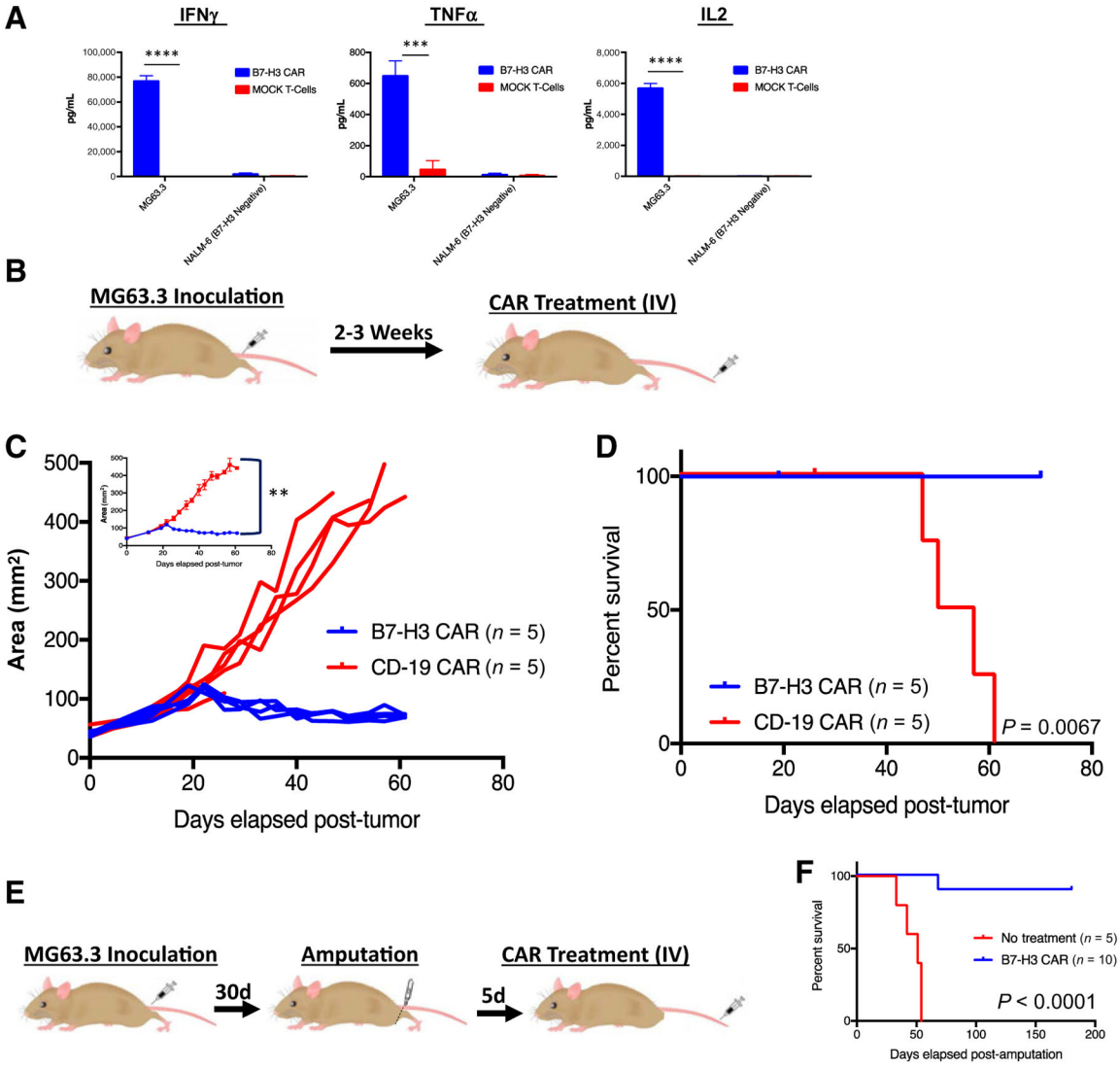

Figure 2.

Systemically administered B7-H3 CAR T cells induce regression of osteosarcoma xenografts. **A**, B7-H3 CAR T cells produce IFNγ, TNFα, and IL2 following 24-hour *in vitro* coculture with MG63.3 osteosarcoma. Representative results of four experiments with 3 different PBMC donors are shown. **B**, Mouse model of orthotopic osteosarcoma: 1e6 MG63.3 tumor cells were injected into the periosteum of the tibia in NSG mice. Two to three weeks later, following onset of measurable tumors, 1e7 B7-H3 CAR^+ T cells or irrelevant control CD19 CAR T cells were intravenously administered. **C**, Tumor growth was measured biweekly by digital caliper and tumor area was calculated. Values for individual mice, as well as mean values per treatment group (inset) are shown. **D**, Survival curves of mice treated as in **B**. Representative results of three experiments with 3 different PBMC donors are shown. **E**, Metastatic model of osteosarcoma: MG63.3-derived tumors were allowed to grow and metastasize before the mouse underwent amputation followed by administration of intravenous 1e7 B7-H3 CAR^+ T cells. **F**, Survival curves of mice treated

as in **E**. Representative results of four experiments with 3 different PBMC donors are shown. Error bars, SEM. *P* values were calculated as described in Materials and Methods.

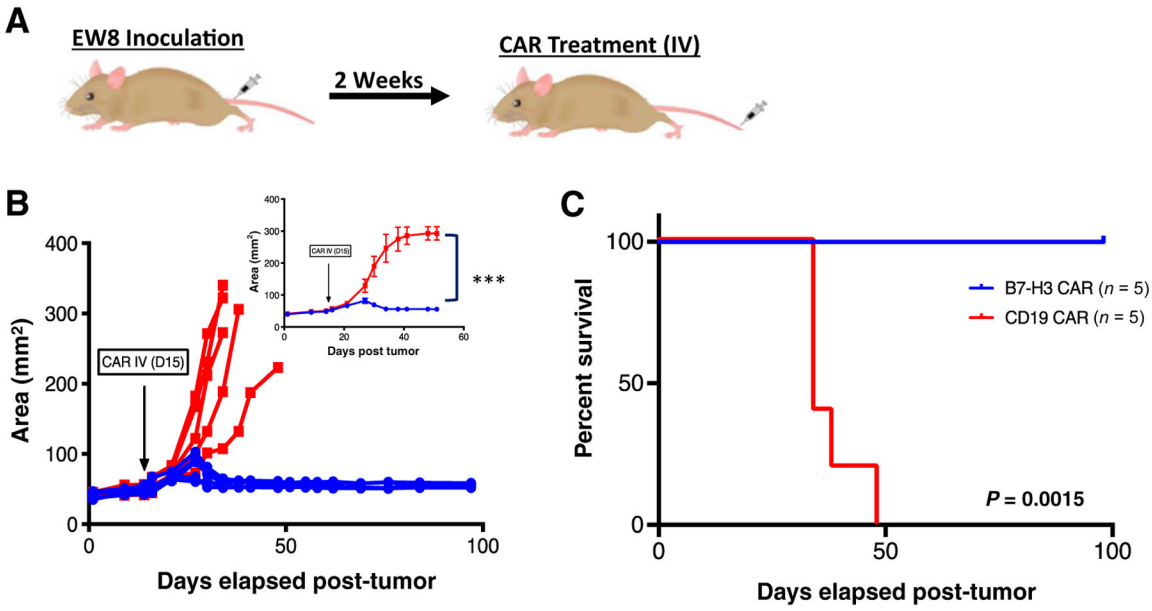

Figure 3.

Systemically administered B7-H3 CAR T cells induce regression of Ewing sarcoma xenografts. **A**, Mouse model of orthotopic Ewing sarcoma: 2e7 EW8 tumor cells were injected into the periosteum of the tibia in NSG mice. Two weeks later, 1e7 B7-H3 CAR$^+$ T cells or irrelevant control CD19 CAR T cells were intravenously administered. **B**, Tumor growth was measured twice weekly by digital caliper and tumor area was calculated. Values for individual mice, as well as mean values per treatment group (inset) are shown. **C**, Survival curves of mice treated as in **A**. Representative results of two experiments with 2 different PBMC donors are shown. Error bars, SEM. *P* values were calculated as described in Materials and Methods.

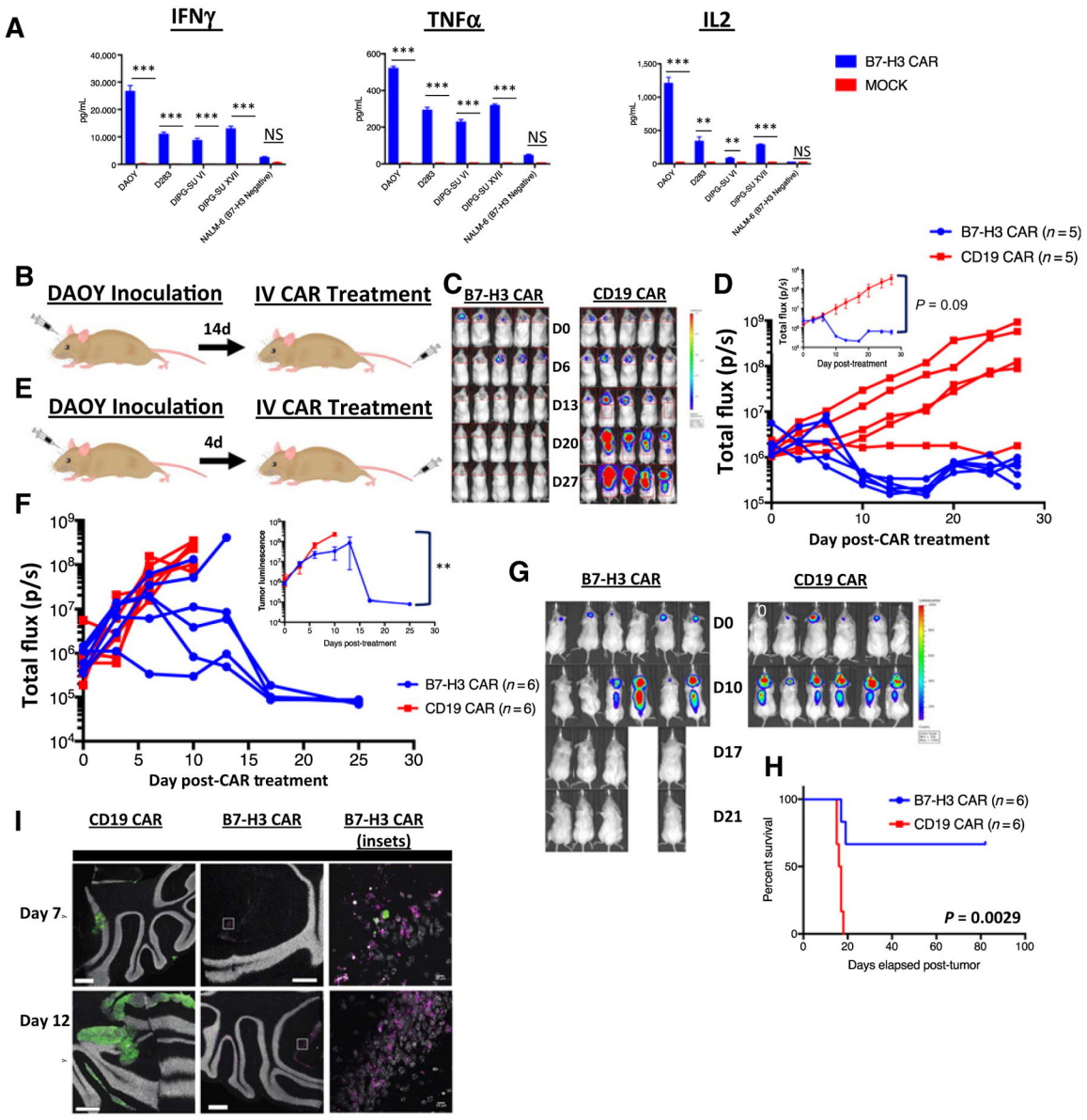

Figure 4.

Systemically administered B7-H3 CAR T cells can clear medulloblastoma xenografts. **A**, B7-H3 CAR T cells were cocultured *in vitro* with medulloblastoma cell lines and patient-derived DIPG cell cultures and, 24 hours later, IFNγ, TNFα, and IL2 were measured in the supernatant. Representative results of three experiments with 3 different PBMC donors are shown. **B**, Orthotopic xenograft model of medulloblastoma: NSG mice were autochthonously injected with luciferase expressing DAOY medulloblastoma tumor cells. Following evidence of tumor engraftment by IVIS imaging, animals received 1e7 B7-H3 CAR$^+$ T cells or CD19 CAR T cells intravenously. **C**, *In vivo* imaging of DAOY tumors treated with B7-H3 or CD19 CAR T cells. **D**, Tumor progression was measured by bioluminescence photometry and flux values (photons per second) were calculated using Living Image software. Values for individual mice, as well as mean values per

treatment group (inset) are shown. Representative results of three experiments with three different PBMC donors are shown. **E**, Orthotopic xenograft model of c-myc–amplified medulloblastoma: D425 tumor cells expressing luciferase were autochthonously injected into NSG mice. Mice were treated with 1e7 B7-H3 CAR^+ T cells or CD19 CAR T cells after 3–4 days, at which point tumor was detectable by IVIS imaging. **F**, Tumor progression was measured by bioluminescence photometry and flux values (photons per second) were calculated using Living Image software. Values for individual mice, as well as average values of living mice per treatment group (inset) are shown. **G**, *In vivo* imaging of D425 tumors treated with B7-H3 or CD19 CAR T cells. **H**, Survival curves of mice shown in **G**. Representative results of three experiments with three different T cell donors are shown. **I**, Confocal images of brains from D425-GFP^+ tumor bearing mice treated with B7-H3 CAR-mCherry or CD19 CAR-mCherry T cells, harvested at two different time points after T-cell infusion. Representative image of two mice at two time points in one experiment. Error bars, SEM. *P* values were calculated as described in Materials and Methods.

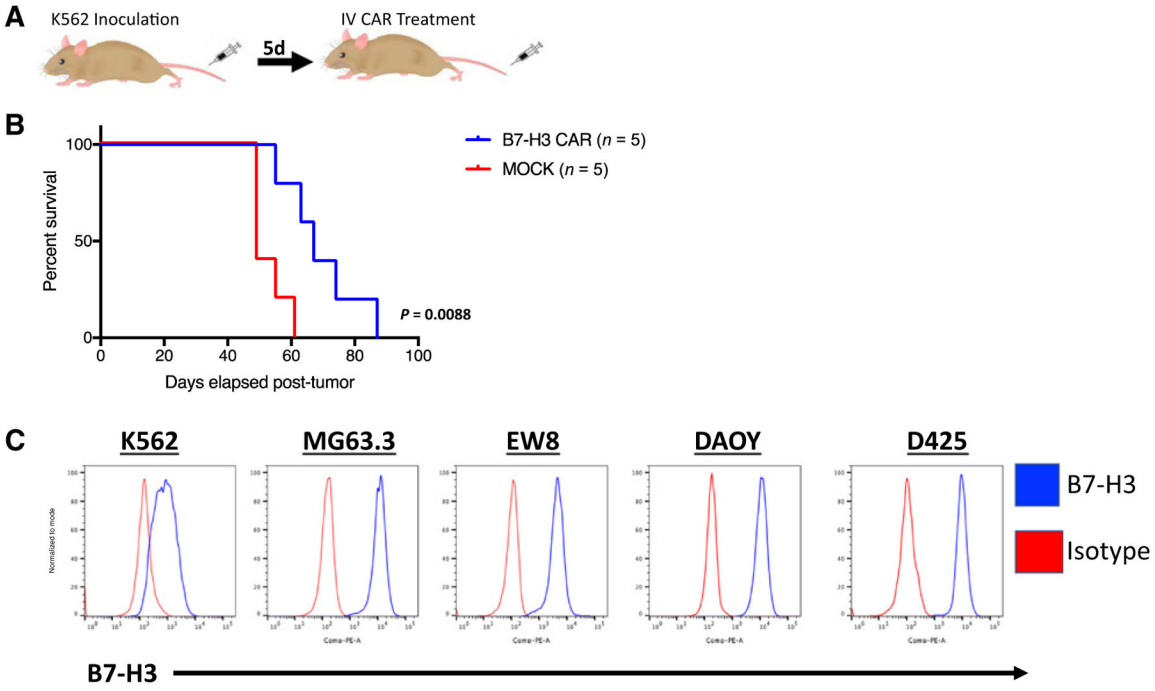

D

Tumor line	Molecules B7-H3/cell
K562	4,750
MG63.3	93,544
EW8	36,260
DAOY	92,050
D425	77,932

Figure 5.

B7-H3 CAR T cells have limited activity against B7-H3 low expressing K562 xenografts. **A**, Mouse model of K562 leukemia: NSG mice were inoculated with K562, a myeloid leukemia that expresses low levels of B7-H3, and then treated with 1e7 B7-H3 CAR$^+$ T cells or mock transduced control T cells 5 days later. **B**, Survival curves of mice treated as in **A**. Representative results of five experiments with three different PBMC donors are shown. **C**, Flow cytometric analysis of B7-H3 expression on the surface of K562 (leukemia), MG63.3 (osteosarcoma), EW8 (Ewing sarcoma), DAOY, and D425 (medulloblastoma) human cell lines. **D**, Number of B7-H3 surface molecules expressed by human tumor cell lines as estimated by Quantibrite kit.

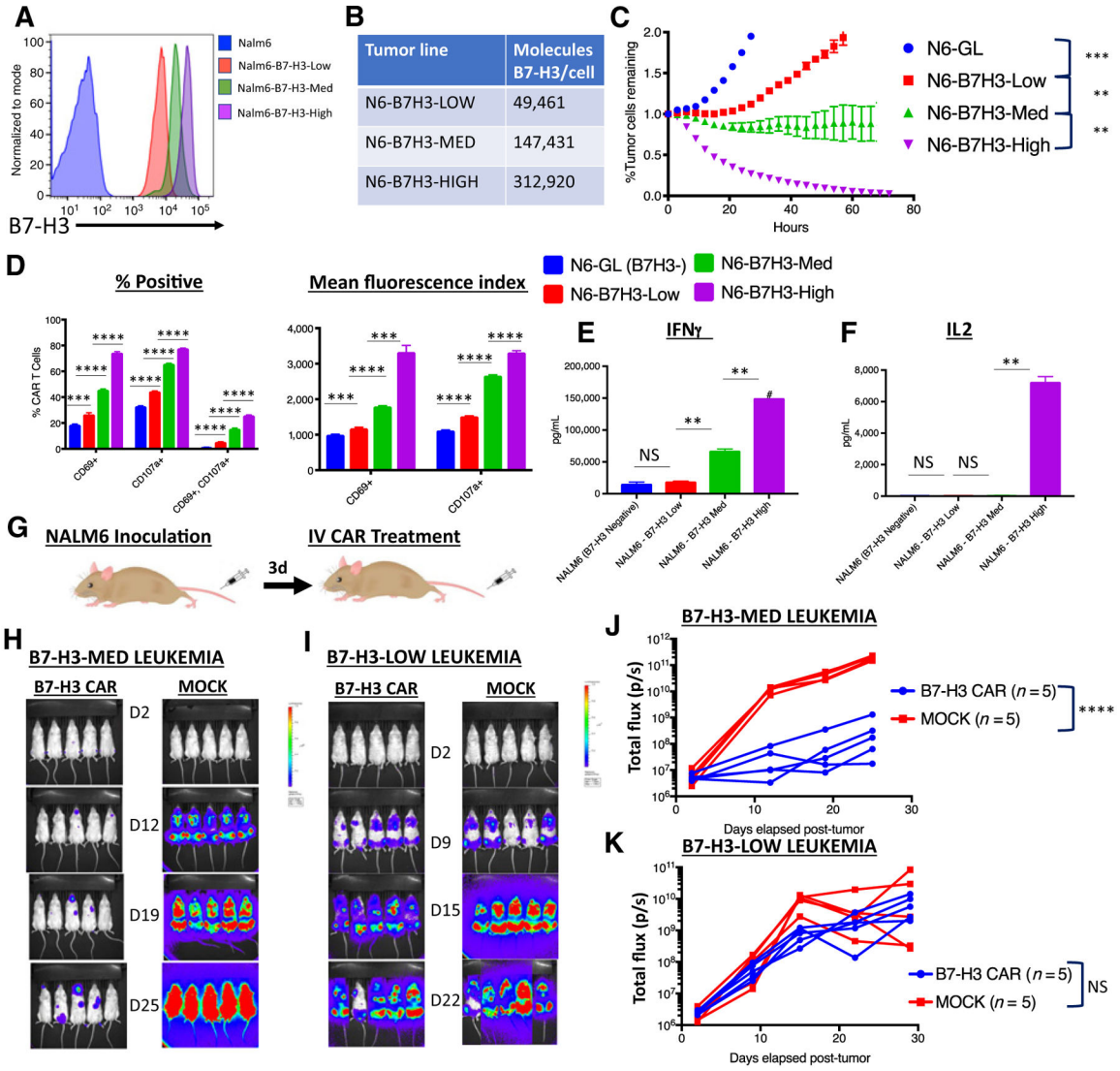

Figure 6.

B7-H3 CAR T cells require adequate antigen expression for *in vitro* and *in vivo* activity. **A**, Flow cytometry analysis of B7-H3 expression on single-cell clones derived from Nalm6 expressing different amounts of lentivirally expressed B7-H3. **B**, Number of B7-H3 surface molecules expressed by Nalm6-B7-H3 cell lines as estimated by Quantibrite kit. **C**, GFP^{+} Nalm6-B7H3 clones were cocultured with B7-H3 CAR T cells and tumor cell killing was measured in an Incucyte assay over 72 hours. Representative data of three experiments with three different PBMC donors is shown. **D**, Percentage of CAR T cells positive (left) and mean fluorescence index (right) for T-cell activation and degranulation markers CD69 and CD107a, as measured by flow cytometry 6 hours after coculture of B7-H3 CAR T cells with tumor cells expressing increasing amounts of B7-H3. Representative results of three experiments with three different PBMC donors are shown. **E** and **F**, Cytokine production by CAR T cells cocultured with tumor cells expressing increasing amounts of B7-H3. **G**, Mouse model for Nalm6-B7H3: 1e6 NALM6 cells expressing either low or medium

amounts of B7-H3 were engrafted into mice by tail vein injection. Three days later, mice were injected with 1e7 B7-H3 CAR^+ T cells or untransduced control T cells (MOCK). *In vivo* imaging of mice bearing (**H**) Nalm6-B7-H3-Medium leukemia or (**I**) Nalm6-B7-H3-Low leukemia. **J** and **K**, Tumor progression was measured by bioluminescence photometry and flux values (photons per second) were calculated using Living Image software. Values for individual mice are shown. Representative results of four (Nalm6-B7-H3-Med) and two (Nalm6-B7-H3-Low) experiments with two different PBMC donors are shown. N6, NALM6; GL, GFP-Luciferase.

Table 1.

Expression of B7-H3 on pediatric tumors by IHC

			Intensity			
Tumor type	**# Stained**	**Positive (%)**	**3+ (%)**	**2+ (%)**	**1+ (%)**	**0 (%)**
Alveolar rhabdomyosarcoma	12	92%	25%	50%	17%	8%
Embryonal rhabdomyosarcoma	10	100%	40%	60%	0%	0%
Ewing sarcoma family of tumors	27	89%	30%	15%	44%	11%
Wilms tumor	12	100%	67%	33%	0%	0%
Neuroblastoma	186	82%	28%	29%	25%	18%
Ganglioneuroblastoma	25	60%	8%	4%	48%	40%
Ganglioneuroma	11	36%	0%	9%	27%	64%
Medulloblastoma	46	96%	61%	22%	13%	4%
High-grade glioma (WHO grade 3/4)	37	84%	35%	16%	33%	16%
Diffuse intrinsic pontine glioma	22	100%	45%	32%	23%	0%
Total	388	84%	34%	25%	25%	16%